Available online at www.sciencedirect.com
SCIENCE DIRECT®
Composites Science and Technology 63 (2003) 2265–2275
COMPOSITES SCIENCE AND TECHNOLOGY
www.elsevier.com/locate/compscitech

Non-linear analysis of the curved shapes of unsymmetric laminates accounting for slippage effects

Maenghyo Cho*, Hee Yuel Roh

School of Mechanical and Aerospace Engineering, Seoul National University, Shinlim-Dong, San 56-1, Kwanak-ku, Seoul, 151-742, South Korea

Received 8 July 2002; received in revised form 19 March 2003; accepted 9 April 2003

Abstract

The shape of unsymmetric laminates at room temperature has an out-of-plane deformation after autoclave curing processing. Unsymmetric cross-ply laminates show two stable curvature shapes because of snap-through when the side lengths of laminates are over a critical value. The shapes of the unsymmetric laminates at room temperature are influenced by various environmental factors such as temperature and moisture. Experiments show a significant effect of tool-plate, which cannot be ignored, on the cured shape of an unsymmetric laminate. We developed the simplified higher-order plate theory for laminates with linear transverse shear profile by applying the Rayleigh-Ritz approximation in the solution procedure. For a refined approximation, in-plane strains were expanded to complete fifth order polynomials. The slippage effects resulting from the interaction between the laminates and the tool-plate were considered. A dimensionless slippage coefficient was introduced, which was correlated to the asymptotic curvature value of the model corresponding experimental one was introduced, and the effect of processing parameters were studied. The previous models, which had been applied only to a square plate, were extended to predict curvatures of rectangular plate configurations with various aspect ratios. The slippage coefficient obtained from the square laminates can be used directly without modification to predict curvatures of rectangular plates with various aspect ratios.

Keywords: A. Polymer-matrix composites (PMCs); B. Non-linear behavior; C. Laminate theory

1. Introduction

Advanced composite structures are manufactured mostly by the autoclave or press-process. During this process, the shapes of laminates change because the elastic moduli and thermal expansion coefficients mismatch between plies. Specifically, the mismatch in the thermal expansion coefficient between plies with different fiber orientation generates residual stresses during the cooling and curing process. These residual stresses causes bending–stretching and bending–twisting couplings, which tend to change the shapes of the unsymmetric laminates from flat plates to curved plates. These stresses may also reduce initial failure strengths of laminates. Thus, the cured shape must be accurately predicted to estimate the residual stresses.

The stable shapes of unsymmetric cross-ply laminates depend upon the size of the plate specimen. Small-squared laminates are saddle shaped. As the size of the plate increases, the stable deformation shape changes from saddle to cylindrical and enters two stable equilibrium states, known as the ''snap-through phenomenon''. Fig. 1 shows the feasible curvature shapes of unsymmetric cross-ply laminates at room temperature. Fig. 1(a) shows flat configurations at a stress-free temperature, which is assumed to be near the glass transition temperature. Fig. 1(b)–(d) show several types of room-temperature shape after cooling down. Fig. 1(b) shows the saddle shape of cross-ply laminates. The CLT (Classical Lamination Theory) [1,2] predicts only this type of room-temperature shape. The CLT predicts neither the curvature shape change due to the size effects nor the snap-through behavior. The snap-through action produces either the shape of Fig. 1(d) or the state of Fig. 1 (c).

Several analyses have been proposed to predict the cured shapes of unsymmetric laminates at room temperature. Originally, Hyer [1–3] and Hamamoto and Hyer [4] developed a nonlinear model based on the von Karman plate theory. This model can predict the snap-through phenomenon and curvature shapes qualitatively, including branch points of curvatures. Hong and

* Corresponding author. Fax: +82-2-883-1513.
E-mail address: mhcho@snu.ac.kr (M. Cho).

0266-3538/03/$ - see front matter © 2003 Elsevier Ltd. All rights reserved.
doi:10.1016/S0266-3538(03)00177-5

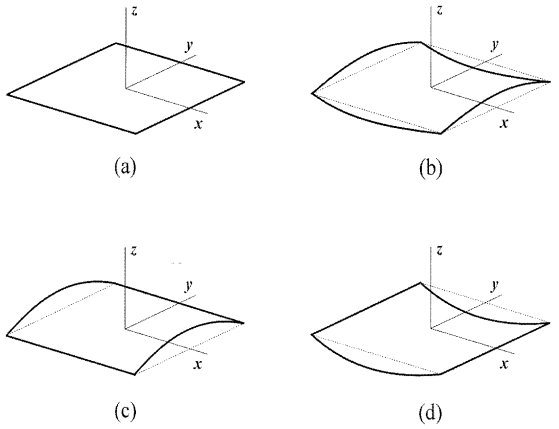

Fig. 1. Geometric shapes with different curvatures at room-temperature.

Jun [5] included an in-plane strain effect in their modeling to account for free-edge effects. Peeters et al. [6] reviewed several theoretical models that could predict curvature shapes of unsymmetric laminates. Schlecht et al. [7] and Schlecht and Schulte [8] employed the finite element methode for the calculation of the room-temperature shapes of unsymmetric laminates. Using the FEA, the geometry of laminate and the lay-up sequence can be modeled easily. Recently, Dano and Hyer [9] proposed a refined model by expanding the complete cubic polynomial for the in-plane normal strain and constant out-of-plane curvatures. However, this model is not adequate to find the convergent solution of room-temperature curvature shapes. An accurate prediction of curvature shapes requires a more refined model.

The predictions of previously proposed models differ from experimental data because the autoclave process exerts various environmental factors on the laminates. To investigate the factors that cause the difference between model predictions and experimental results, Cho et al. [8] proposed a higher-order plate model with von Karman nonlinearity to account for the environment factors. Instead of modeling each factor individually, they introduced a dimensionless slippage coefficient to investigate global effects of processing parameters. However, the third-order shear deformation model they developed is not adequate to describe the slippage effect because the transverse shear stress profile through the thickness of laminates does not show a monotonic pattern in the thickness direction. Thus, the model needed to be corrected to reliably predict the room-temperature curvature shapes. They used the Rayleigh-Ritz approximation in the solution procedure and a cubic polynomial as the basis function for the in-plane displacement field. However, this cubic polynomial does not accurately predict the curvature shape of the laminates after it has been cooled to room temperature.

In the present study, we use the slippage model proposed by Cho et al. [10] to predict the room-temperature curvature shapes. To produce a monotonically varying transverse shear stress profile through the thickness of the laminates, a quadratic higher-order plate model was developed and the previous cubic model was not used. In addition, to obtain the higher precision Rayleigh-Ritz approximate solutions, a fifth-order polynomial basis function was employed on the in-plane normal strain field instead of the cubic polynomial basis functions for the in-plane displacement field as was used in the previous study. The model previously applied only to the square plates was extended to predict curvature of unsymmetric rectangular laminates of various aspect ratios.

2. Formulation

2.1. Displacements, strains, and slippage modeling

In the model of Hamamoto and Hyer [4], the displacement fields that predicted the curved shape with snap-through for the unsymmetric laminates are based on the CLT with von Karman geometric non-linearity. But since their model does not include the transverse shear strain, the transverse shear stress resulting from slippage between laminates and tool-plate cannot be included. In our present study, the displacement fields that account for the slippage effect were based on simplified higher-order theory,

$$\begin{aligned} u_1(x,y,z) &= u_1^0(x,y) + \varphi_1 z + \xi_1 z^2 \\ u_2(x,y,z) &= u_2^0(x,y) + \varphi_2 z + \xi_2 z^2 \\ u_3(x,y,z) &= w(x,y) \end{aligned} \tag{1}$$

The schematic of the laminate and tool plate and the profile of the transverse shear stresses are given in Fig. 2. The boundary conditions of transverse shear stress at the top and bottom surfaces of laminates are given as follows.

$$\begin{aligned} &z = h/2 : \sigma_{32} = \sigma_{31} = 0 \\ &z = -h/2 : \sigma_{32} = \beta_2 T_2, \sigma_{31} = \beta_1 T_1 \end{aligned} \tag{2}$$

T_1 and T_2 are transverse shear stresses in the x and y directions, respectively, at the boundary surface. The dimensionless coefficients β_1 and β_2 indicate the degree of slippage. The terms of $\beta_\alpha T_\alpha$ ($\alpha = 1, 2$) indicate transverse shear stresses due to slip between the laminates and the tool-plate. The interaction between tool-plate and laminate will be referred to as a "slippage effect". It produces transverse shear stress across the thickness of the laminates, which reduces the curvature after cooling, as shown in Fig. 2. To express the variables $\beta_\alpha T_\alpha$ in terms of the quantities related to the bending moment resultants, one must consider the effects of transverse shear stress on the curvature shape. These mechanisms are modeled in Fig. 3. When flat laminates are cured at high temperature and cooled down to room temperature, the flat laminates change to curved laminates and this change is directly related to the moment

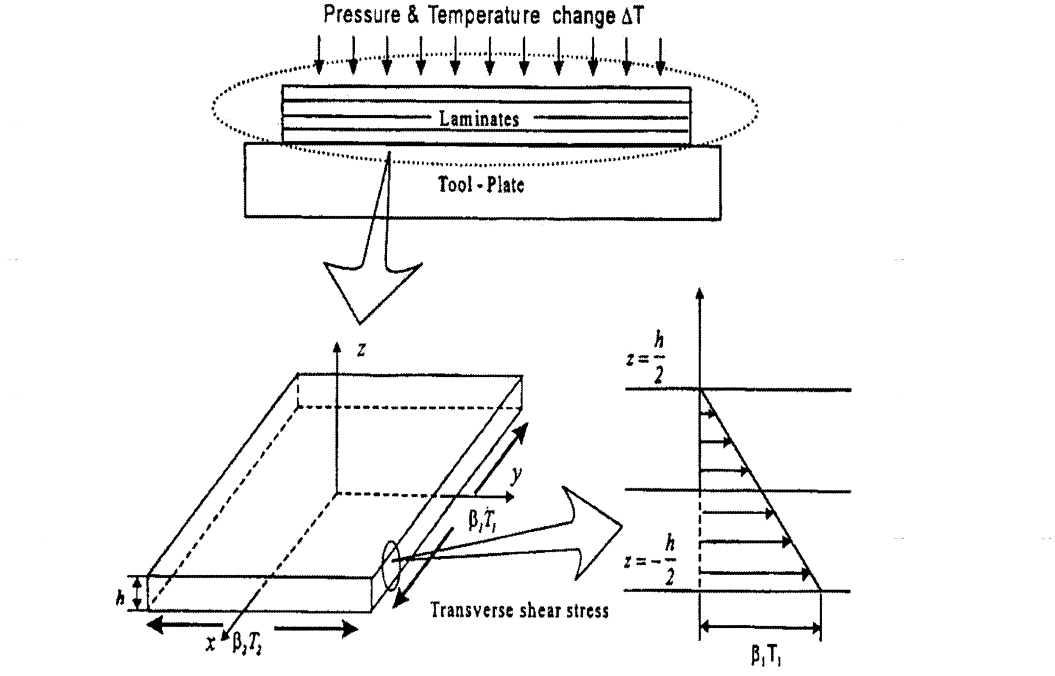

(a) Present model

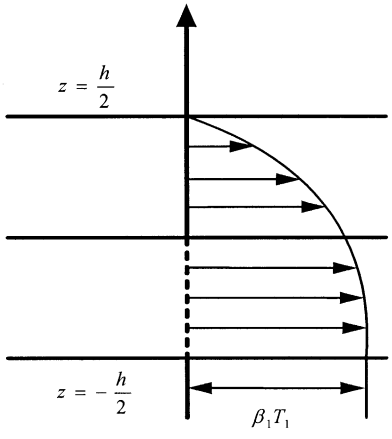

(b) Previous model [8]

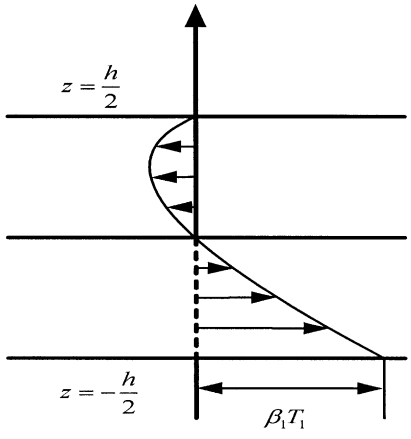

(c) Unrealistic transverse shear distribution of the previous model[8]

Fig. 2. Transverse shear stress boundary conditions.

resultants,M_1 and M_2. The moment resultants M_1 and M_2 are calculated from the following relationships.

$$\begin{Bmatrix} N \\ M \end{Bmatrix} = \begin{bmatrix} A & B \\ C & D \end{bmatrix} \begin{Bmatrix} \varepsilon^0 \\ \kappa \end{Bmatrix} \tag{3}$$

Fig. 3(a) shows a deformed post-curing configuration that did not consider the slippage effects. M_α^* indicates the moment resultants that generate curvature at room temperature. M_α is the moment resultant that generates the actual shape of curved laminate at room temperature. Because the slippage effects were not considered, the values of the resultant moments M_α and M_α^* were equal in Fig. 3(a).

Fig. 3(b) shows the case in which the curvature decreased because of slippage effects. Since this effects change the moment resultants from M_α to M_α^*, the following moment equilibrium equations associated with laminate equilibrium configurations should be satisfied:

$$\int_{-L_x/2}^{L_x/2}\beta_1 T_1 \mathrm{d}x\frac{h}{2} = 2\left(M_1^* - M_1\right) = 2\beta_1^* M_1$$
$$\int_{-L_y/2}^{L_y/2}\beta_2 T_2 \mathrm{d}y\frac{h}{2} = 2\left(M_2^* - M_2\right) = 2\beta_2^* M_2 \tag{4}$$

where the change of moment resultants $(M_\alpha - M_\alpha^*)$ are approximated as $\beta_\alpha^* M_\alpha$, with the introduction of coefficients β_α^*. The transverse shear stresses $\beta_\alpha T_\alpha$ are assumed uniform over the surface of the laminates. The transverse shear stresses may be approximated as follows:

$$\beta_1 T_1 \approx \frac{4}{L_x h} D_{11}\beta_1^* a$$
$$\beta_2 T_2 \approx \frac{4}{L_y h} D_{22}\beta_2^* b \tag{5}$$

Fig. 3(c) is the ideal critical case, in which the deformed curvature shape of laminates after curing is nearly flat because of the excessively applied slippage effect. The coefficient β_α^* reaches the critical value $\beta_{\alpha\mathrm{cr}}^*$. The critical value $\beta_{\alpha\mathrm{cr}}^*$ is equal to 1, at which curvatures have zero asymptotic values.

Dimensionless coefficients $\beta_1$and β_2 ranging from 0 to 1 for cross-ply laminate are given by the following equations.

$$\beta_1 = \frac{\beta_1^*}{\beta_{\mathrm{cr}}^*}, \quad \beta_2 = \frac{\beta_2^*}{\beta_{\mathrm{cr}}^*} \tag{6}$$

Thus, when β is equal to 0, the results are the same as Hyer's, in which slippage effects are ignored. On the other hand, when β is equal to 1, the laminates remain flat after curing.

Transverse shear strains are then given by:

$$\begin{Bmatrix}\gamma_{32}\\ \gamma_{31}\end{Bmatrix} = \begin{Bmatrix}\frac{\partial u_1}{\partial z}+\frac{\partial u_3}{\partial x}\\ \frac{\partial u_2}{\partial z}+\frac{\partial u_3}{\partial y}\end{Bmatrix} = \frac{1}{Q_{44}Q_{55}-Q_{45}^2}\begin{bmatrix}Q_{55} & -Q_{45}\\ -Q_{45} & Q_{44}\end{bmatrix}\begin{Bmatrix}\sigma_{32}\\ \sigma_{31}\end{Bmatrix} \tag{7}$$

The four dependent variables φ_1, φ_2, ξ_1 and ξ_2 are subject to the surface boundary conditions given in Eq. (2). The four dependent variables can be determined as follows.

$$\varphi_1 = \frac{1}{2}\frac{Q_{44}\beta_1 T_1 - Q_{45}\beta_2 T_2}{Q_{44}Q_{55}-Q_{45}^2} - \frac{\partial w}{\partial x}$$
$$\varphi_2 = \frac{1}{2}\frac{Q_{55}\beta_2 T_2 - Q_{45}\beta_1 T_1}{Q_{44}Q_{55}-Q_{45}^2} - \frac{\partial w}{\partial y}$$
$$\xi_1 = -\frac{1}{2h}\frac{Q_{44}\beta_1 T_1 - Q_{45}\beta_2 T_2}{Q_{44}Q_{55}-Q_{45}^2}$$
$$\xi_2 = -\frac{1}{2h}\frac{Q_{55}\beta_2 T_2 - Q_{45}\beta_1 T_1}{Q_{44}Q_{55}-Q_{45}^2} \tag{8}$$

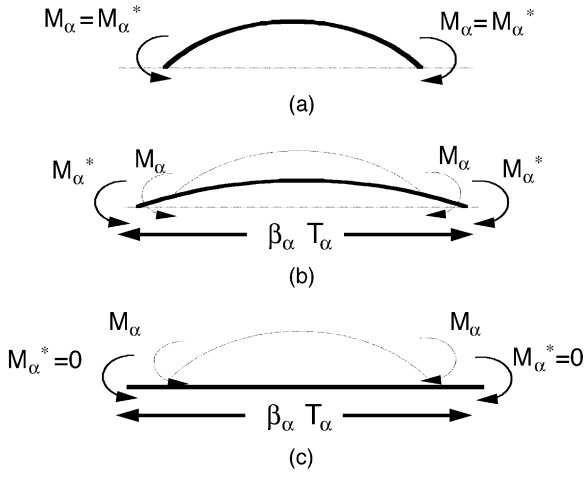

Fig. 3. Modeling to determine slippage coefficient β_α.

Substituting Eq. (8) into Eq. (1), the final displacement fields satisfying transverse shear stress boundary conditions at the top and bottom surfaces are obtained.

$$u_1 = u_1^0 - \frac{\partial w}{\partial x}z + \frac{z}{2}\frac{Q_{44}\beta_1 T_1 - Q_{45}\beta_2 T_2}{Q_{44}Q_{55}-Q_{45}^2} - \frac{z^2}{2h}\frac{Q_{44}\beta_1 T_1 - Q_{45}\beta_2 T_2}{Q_{44}Q_{55}-Q_{45}^2}$$
$$u_2 = u_2^0 - \frac{\partial w}{\partial y}z + \frac{z}{2}\frac{Q_{55}\beta_2 T_2 - Q_{45}\beta_1 T_1}{Q_{44}Q_{55}-Q_{45}^2} - \frac{z^2}{2h}\frac{Q_{55}\beta_2 T_2 - Q_{45}\beta_1 T_1}{Q_{44}Q_{55}-Q_{45}^2} \tag{9}$$

As shown in Fig. 2, the transverse shear stresses due to slippage effects were modeled as a linear function through the thickness. On the other hand, in the previous study [10], the in-plane displacement is assumed to be cubic and the transverse shear stress distribution is assumed to be parabolic through the thickness. The displacement field and transverse shear strain proposed in Ref. [10] are shown below.

$$u_1 = u_1^0 - \frac{\partial w}{\partial x}z - \frac{z^2}{2h}\frac{Q_{44}\beta_1 T_1 - Q_{45}\beta_2 T_2}{Q_{44}Q_{55}-Q_{45}^2} - \frac{2z^3}{3h^2}\frac{Q_{44}\beta_1 T_1 - Q_{45}\beta_2 T_2}{Q_{44}Q_{55}-Q_{45}^2}$$
$$u_2 = u_2^0 - \frac{\partial w}{\partial y}z - \frac{z^2}{2h}\frac{Q_{55}\beta_2 T_2 - Q_{45}\beta_1 T_1}{Q_{44}Q_{55}-Q_{45}^2} - \frac{2z^3}{3h^2}\frac{Q_{55}\beta_2 T_2 - Q_{45}\beta_1 T_1}{Q_{44}Q_{55}-Q_{45}^2} \tag{10}$$
$$\gamma_{yz} = \frac{\partial u_2}{\partial z}+\frac{\partial w}{\partial y} = \frac{z(2z-h)}{h^2}\frac{Q_{55}\beta_2 T_2 - Q_{45}\beta_1 T_1}{Q_{44}Q_{55}-Q_{45}^2}$$
$$\gamma_{xz} = \frac{\partial u_1}{\partial z}+\frac{\partial w}{\partial x} = \frac{z(2z-h)}{h^2}\frac{Q_{44}\beta_1 T_1 - Q_{45}\beta_2 T_2}{Q_{44}Q_{55}-Q_{45}^2}$$

However, the parabolic profile leads to an unrealistic pattern of the transverse shear stresses across the thickness. This unrealistic transverse shear stress profile is depicted in Fig. 2.

We assume a simple linear distribution of the transverse shear deformation through the thickness. The approximate analysis is based on a Rayleigh-Ritz minimization of the total potential energy. The displacement functions obtained in Eq. (9) and Eq. (1) are used to derive the expressions for their corresponding strains needed to compute the laminate strain energy. Thus, rather than the displacement fields, the laminate mid-plane strains were expanded.

The mid-plane strains accounting for geometric von Karman non-linearity are expressed as:

$$\begin{aligned}\varepsilon_x^0 &= \frac{\partial u_1^0}{\partial x} + \frac{1}{2}\left(\frac{\partial w^0}{\partial x}\right)^2 \\ \varepsilon_y^0 &= \frac{\partial u_2^0}{\partial y} + \frac{1}{2}\left(\frac{\partial w^0}{\partial y}\right)^2 \\ \gamma_{xy}^0 &= \frac{\partial u_1^0}{\partial y} + \frac{\partial u_2^0}{\partial x} + \left(\frac{\partial w^0}{\partial x}\right)\left(\frac{\partial w^0}{\partial y}\right)\end{aligned} \tag{11}$$

The in-plane normal strains were expanded as complete fifth-order polynomials to obtain the convergent reference solution, and the out-of-plane deflection was assumed to be a complete quadratic polynomial equation, which was used to generate constant curvature as shown in Fig. 4.

The fifth-order mid-plane strains and out-of-plane displacement are given as follows:

$$\begin{aligned}\varepsilon_x^0 &= c_{00} + c_{10}x + c_{01}y + c_{20}x^2 + c_{11}xy + c_{02}y^2 \\ &\quad + c_{30}x^3 + c_{21}x^2y + c_{12}xy^2 + c_{03}y^3 + c_{40}x^4 \\ &\quad + c_{31}x^3y + c_{22}x^2y^2 + c_{13}xy^3 + c_{04}y^4 + c_{50}x^5 \\ &\quad + c_{41}x^4y + c_{32}x^3y^2 + c_{23}x^2y^3 + c_{14}xy^4 + c_{05}y^5 \\ \varepsilon_y^0 &= d_{00} + d_{10}x + d_{01}y + d_{20}x^2 + d_{11}xy + d_{02}y^2 \\ &\quad + d_{30}x^3 + d_{21}x^2y + d_{12}xy^2 + d_{03}y^3 + d_{40}x^4 \\ &\quad + d_{31}x^3y + d_{22}x^2y^2 + d_{13}xy^3 + d_{04}y^4 + d_{50}x^5 \\ &\quad + d_{41}x^4y + d_{32}x^3y^2 + d_{23}x^2y^3 + d_{14}xy^4 + d_{05}y^5 \\ w^0(x,y) &= \frac{1}{2}(ax^2 + cxy + by^2)\end{aligned} \tag{12}$$

The total strains in the laminates are given by

$$\begin{aligned}&\varepsilon_x = \varepsilon_x^0 + z\kappa_x^0, \quad \varepsilon_y = \varepsilon_y^0 + z\kappa_y^0, \quad \gamma_{xy} = \gamma_{xy}^0 + z\kappa_{xy}^0 \\ &\gamma_{yz} = \frac{\partial u_2}{\partial z} + \frac{\partial w}{\partial y} = \left(\frac{1}{2} - \frac{z}{h}\right)\frac{Q_{55}\beta_2 T_2 - Q_{45}\beta_1 T_1}{Q_{44}Q_{55} - Q_{45}^2} \\ &\gamma_{xz} = \frac{\partial u_1}{\partial z} + \frac{\partial w}{\partial x} = \left(\frac{1}{2} - \frac{z}{h}\right)\frac{Q_{44}\beta_1 T_1 - Q_{45}\beta_2 T_2}{Q_{44}Q_{55} - Q_{45}^2}\end{aligned} \tag{13}$$

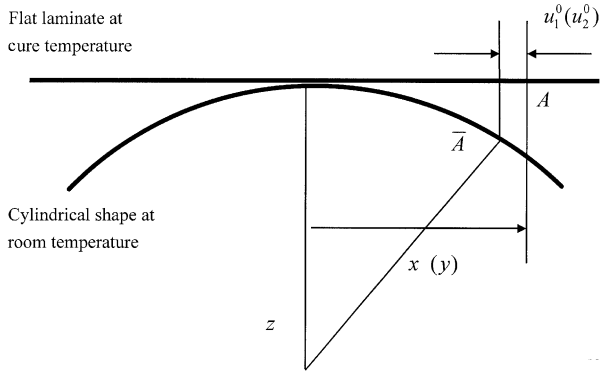

Fig. 4. Cylindrical curvature shape of an unsymmetric laminate plate.

where ε_x^0, ε_y^0 and γ_{xy}^0 are the laminate mid-plane strains and κ_x^0, κ_y^0 and κ_{xy}^0 are the mid-plane curvatures in the x- and y-directions and the twist curvature, respectively. The mid-plane curvatures are defined by

$$\begin{aligned}&\kappa_x^0 = -\frac{\partial^2 w^0}{\partial x^2} = -a, \qquad \kappa_y^0 = -\frac{\partial^2 w^0}{\partial y^2} = -b, \\ &\kappa_{xy}^0 = -2\frac{\partial^2 w^0}{\partial x \partial y} = -c\end{aligned} \tag{14}$$

The in-plane displacements u_1^0 and u_2^0 can be obtained by integrating the strain-displacement equations with von Karman non-linearity.

$$\begin{aligned}u_1^0 &= \int\left\{\varepsilon_x^0 - \frac{1}{2}\left(\frac{\partial w^0}{\partial x}\right)^2\right\}\mathrm{d}x + g(y) \\ u_2^0 &= \int\left\{\varepsilon_y^0 - \frac{1}{2}\left(\frac{\partial w^0}{\partial y}\right)^2\right\}\mathrm{d}y + h(x)\end{aligned} \tag{15}$$

The in-plane shear strain γ_{xy}^0 is obtained by substituting Eq. (12) and Eq. (15) into Eq. (16).

$$\gamma_{xy}^0 = \frac{\partial u_1^0}{\partial y} + \frac{\partial u_2^0}{\partial x} + \left(\frac{\partial w^0}{\partial x}\right)\left(\frac{\partial w^0}{\partial y}\right) \tag{16}$$

Transverse shear strains in Eq. (13) now can be expressed as functions of generalized coordinates a, b and c by using Eq. (5).

2.2. Minimization of total potential energy

The deformed shapes after curing are in a state of equilibrium in which the total potential energy inside the body is at minimum. Assuming a plane stress state, the strain energy density function of the laminate, ψ, can be expressed in the following form, and the total potential energy is represented as the volume integral of the strain energy density function.

$$\psi = \frac{1}{2}\begin{Bmatrix}\varepsilon_x\\ \varepsilon_y\\ \gamma_{xy}\end{Bmatrix}^T\begin{bmatrix}Q_{11} & Q_{12} & Q_{16}\\ Q_{12} & Q_{22} & Q_{26}\\ Q_{16} & Q_{26} & Q_{66}\end{bmatrix}^{(k)}\begin{Bmatrix}\varepsilon_x\\ \varepsilon_y\\ \gamma_{xy}\end{Bmatrix} + \frac{1}{2}\begin{Bmatrix}\gamma_{yz}\\ \gamma_{xz}\end{Bmatrix}^T\begin{bmatrix}Q_{44} & Q_{45}\\ Q_{45} & Q_{55}\end{bmatrix}^{(k)}\begin{Bmatrix}\gamma_{yz}\\ \gamma_{xz}\end{Bmatrix} - \begin{Bmatrix}\varepsilon_x\\ \varepsilon_y\\ \gamma_{xy}\end{Bmatrix}^T \begin{bmatrix}Q_{11} & Q_{12} & Q_{16}\\ Q_{12} & Q_{22} & Q_{26}\\ Q_{16} & Q_{26} & Q_{66}\end{bmatrix}^{(k)}\begin{Bmatrix}\alpha_x\Delta T\\ \alpha_y\Delta T\\ \alpha_{xy}\Delta T\end{Bmatrix} \tag{17}$$

where ΔT is the applied temperature and the $[Q_{ij}]^{(k)}$ is the transformed reduced stiffness matrix of the k-th layer.

Back-substituting the mid-plane strains and curvatures into the total strains, Eq. (9), and into the definition of the total potential energy, Eq. (17), the final result is an algebraic expression for the total potential energy of the laminate of the form

$$\Pi = \iiint_v \psi \mathrm{d}x\mathrm{d}y\mathrm{d}z = \Pi(a, b, c, c_{00}, c_{10}, c_{01}, \ldots, d_{00}, d_{10}, d_{01}, \ldots, e_1 \ldots e_6) \tag{18}$$

Obviously, Π is also a function of the laminate material properties and geometry, but here interest centers on the unknown coefficients. To study the deformation of the laminate, we used the variation of the total potential energy by equating the first variation to zero and reorganizing the equations by reducing some coefficients between them that obtained by equating the first variation to zero. From the 51 dependent variables given in Eq. (18), the 48 variables out of total 51 variables can be expressed in terms of the remaining three variables a, b, and c through symbolic manipulation provided by the commercial software *Mathematica* [11]. The final results were reduced to three nonlinear algebraic equations with three dependent variables, a, b and c. These equations admit multiple solutions and each solution corresponds to each equilibrium branch. In the present study, the second variation of total potential energy was considered to indicate the stability of the equilibrium path.

3. Numerical results and discussions

The laminates that were used for verification in the present experiment were DMS-2224 manufactured by Hercules Co., and the material properties of the laminates are given as follows.

- Laminates (DMS-2224)

$$E_1 = 104.8\ \text{GPa},\quad E_2 = 8.07\ \text{GPa},$$
$$G_{12} = 4.17\ \text{GPa},\quad G_{13} = G_{12}$$
$$\nu_{12} = 0.33,\quad \alpha_1 = 0.3\times10^{-6}/^\circ\text{C},$$
$$\alpha_2 = 36.5\times10^{-6}/^\circ C$$
$$\Delta T = 150^\circ\text{C},\ \text{lamina thickness} = 0.01397\ \text{cm}$$

- Aluminum: $E = 70$ GPa, $\nu = 0.34$, $\alpha = 2.3\times10^{-5}/^\circ$C
- Rubber: $E = 7\times10^{-4}$GPa, $\nu = 0.5$, $\alpha = 1.3\times10^{-4}/^\circ$C

For calculation convenience, the lamina thickness was assumed to be uniform at each layer. The laminates were heated for 30 min from room temperature up to 177 °C monotonically and cured at 177 °C for 2 h and cooled to room temperature at a cooling rate of 5 °C/min. During this cycle, the autoclave pressure was maintained at 0.586×10^6 Pa. The cured 300×300 mm laminates were cut successively to the smaller square plates to measure the curvature for each length of side. The rectangular plate case also followed the same procedure. The curvature κ was experimentally determined using the relation

$$\kappa = \frac{1}{R} = \frac{8\mathrm{d}}{C^2 + 4\mathrm{d}^2} \tag{19}$$

as depicted in Fig. 5.

The change of curvature for various side lengths of the laminate considering von Karman nonlinearity are depicted and experimental results are compared with analytical solutions obtained by Hyer's theory. The dimensionless coefficients β_1 and β_2 were derived from the correlation of theoretical solutions with the experimental data at one point (side length of laminate = 0.3 m).

Fig. 6 shows the change of curvature shapes of square laminate versus side length. When the side length was smaller than 0.045 m, the shape of the laminate became saddle shaped. On the other hand, when the side length was larger than the critical size (=0.045 m), the curvature shape changed from saddle to the cylindrical pattern. The deformed schematics in Fig. 6 are given to

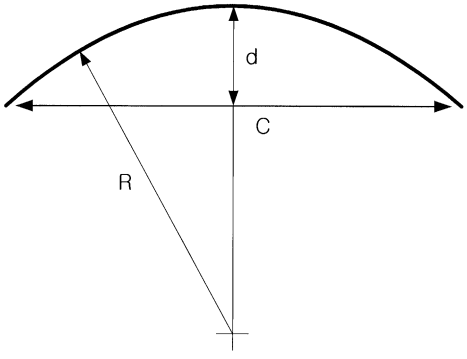

Fig. 5. Measurements of curvature.

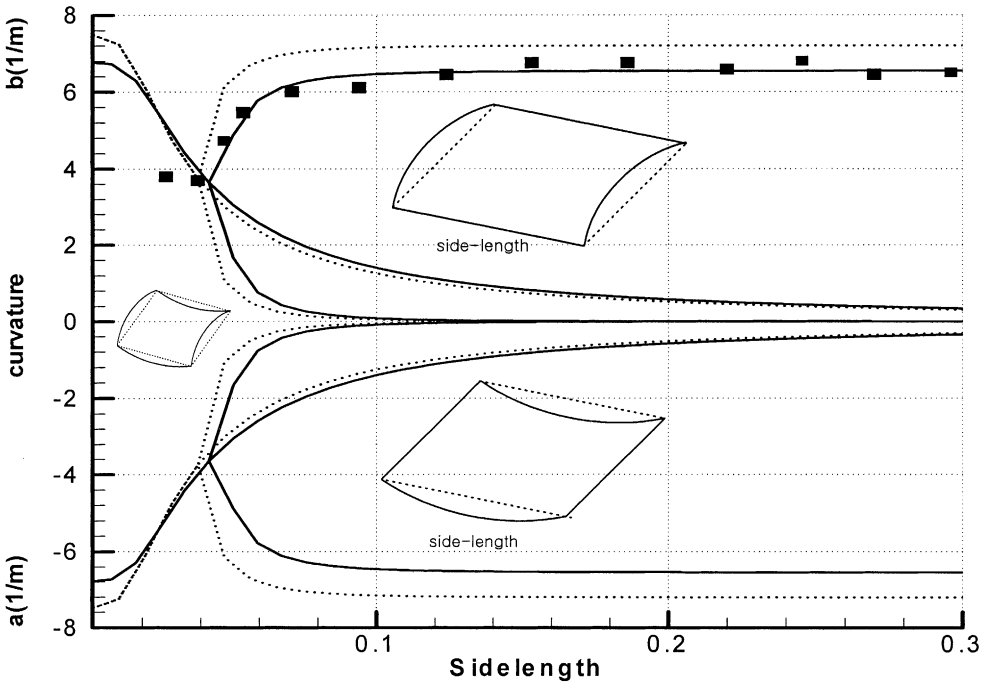

Fig. 6. Change of curvature as a function of the side length for $[0_2/90_2]$ laminate (Smooth Al Tool: $\beta_1 = \beta_2 = 0.055$) [—: Present, ·····: Hyer, ■: Experiment].

illustrate the change of curvature shapes versus the side-length of the laminates. As shown in Fig. 6, though the original Hyer's model predicts the snap-through phenomenon and curvature shapes qualitatively, the curvatures obtained by his method are larger than the experimental results. However, our model using the fifth-order polynomial approximation based on Hyer's model and considering slippage effect agreed better with the experiment data. The results were more accurate than those in Cho et al.'s study [10], because the model was based on the feasible profile of transverse shear distribution across the thickness of laminates and fifth-order complete polynomial approximate was used in the in-plane normal strain assumption. In Fig. 7, the change

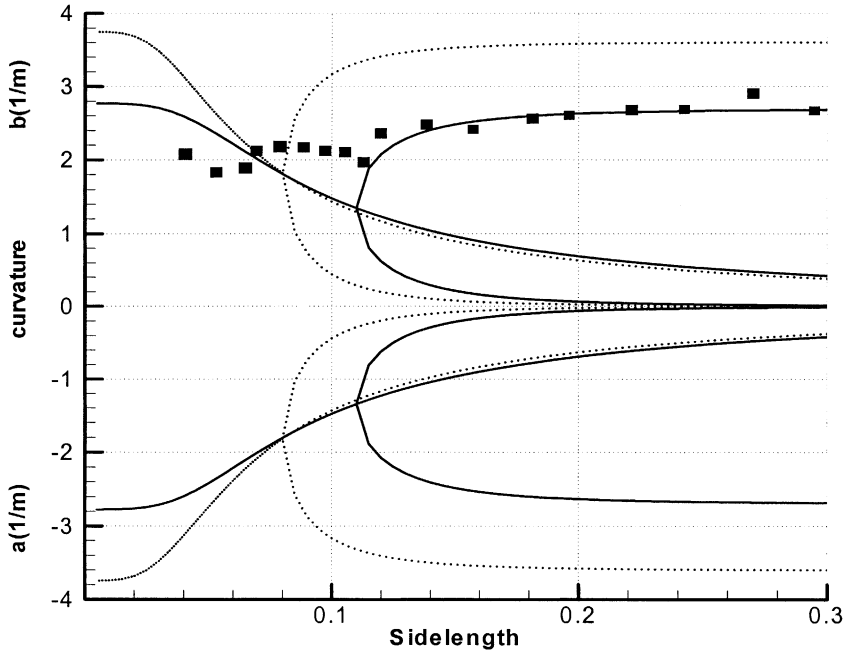

Fig. 7. Change of curvature as a function of the side length for $[0_4/90_4]$ laminate (Smooth Al Tool: $\beta_1 = \beta_2 = 0.11$) [—: Present, ·····: Hyer, ■: Experiment].

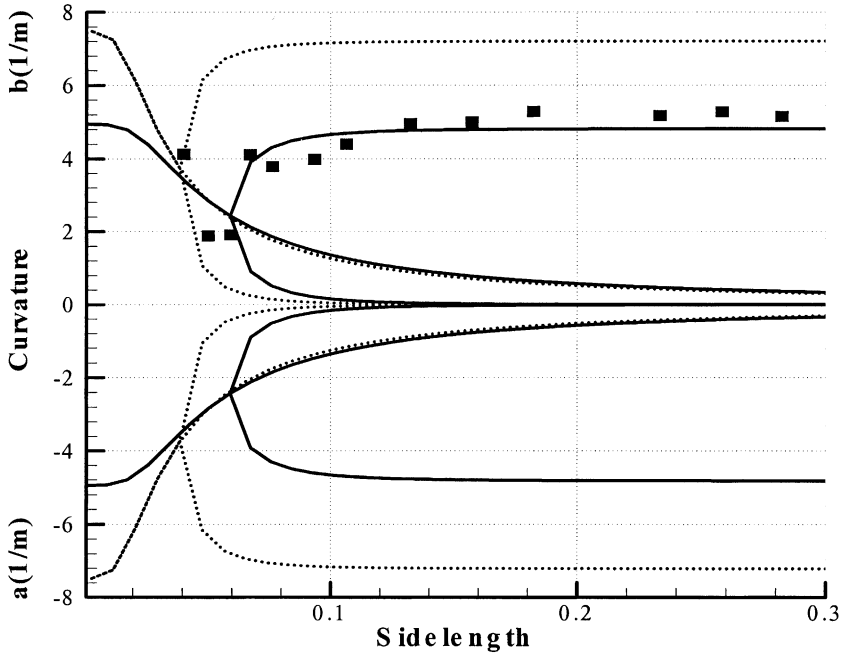

Fig. 8. Change of curvature as a function of the side length for $[0_2/90_2]$ laminate (Rubber Tool: $\beta_1 = \beta_2 = 0.0865$) [—: Present, ·····: Hyer, ■: Experiment].

of curvature of the laminate with $[0_4/90_4]$ cross-ply layup was investigated. As the thickness of laminate increased, the values of the coefficients β_1 and β_2 increased. Moreover, as the number of plies increased, the bifurcation point of curvature moved toward a larger side-length. Accordingly, when the same tool-plate was used and as the thickness of laminate is increased, the coefficients increased and the bifurcation point of curvature moved toward the direction of increasing side-length.

Figs. 8 and 9 show the model predictions and the experimental results for the rubber tool-plate cases. The results show that the matched values of the coefficients β_1 and β_2 were larger than those for the aluminum tool-plate case. These larger values suggest that the curvature was affected by the surface roughness and thermal

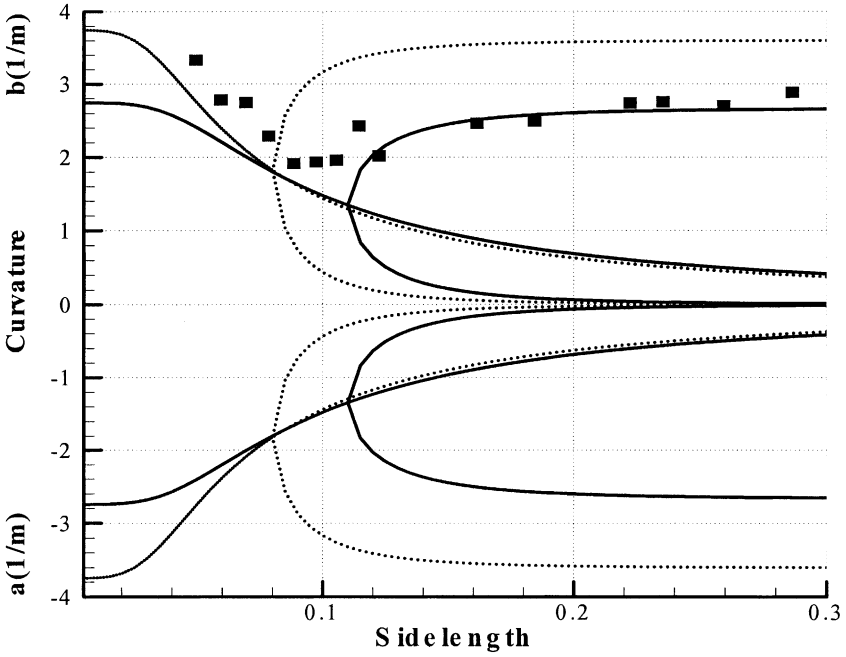

Fig. 9. Change of curvature as a function of the side length for $[0_4/90_4]$ laminate (Rubber Tool: $\beta_1 = \beta_2 = 0.11$) [—: Present, ·····: Hyer, ■: Experiment].

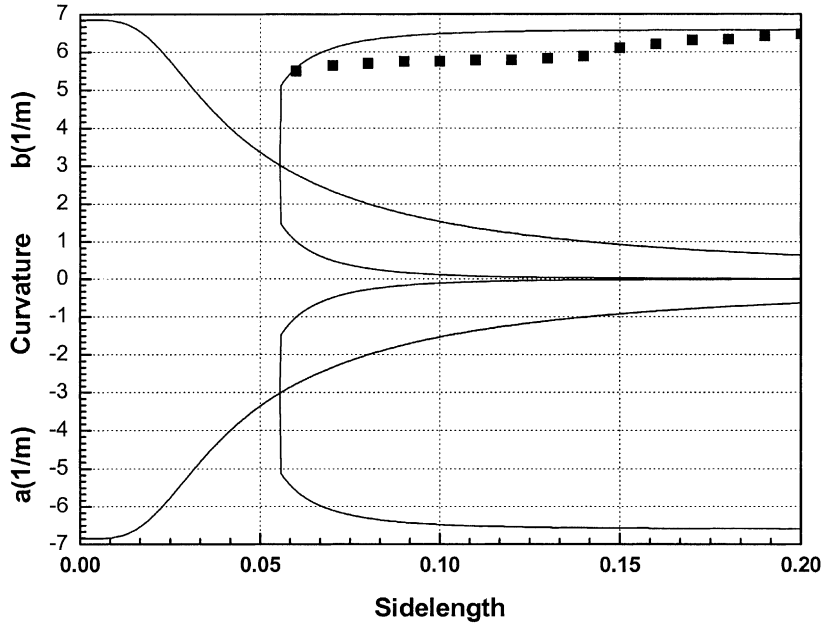

Fig. 10. Change of curvature as a function of the side length for $[0_2/90_2]$ laminate with 0.2×0.2 m (Smooth Al Tool: $\beta_1 = 0.075, \beta_2 = 0.055$) [—: Present, ■: Experiment].

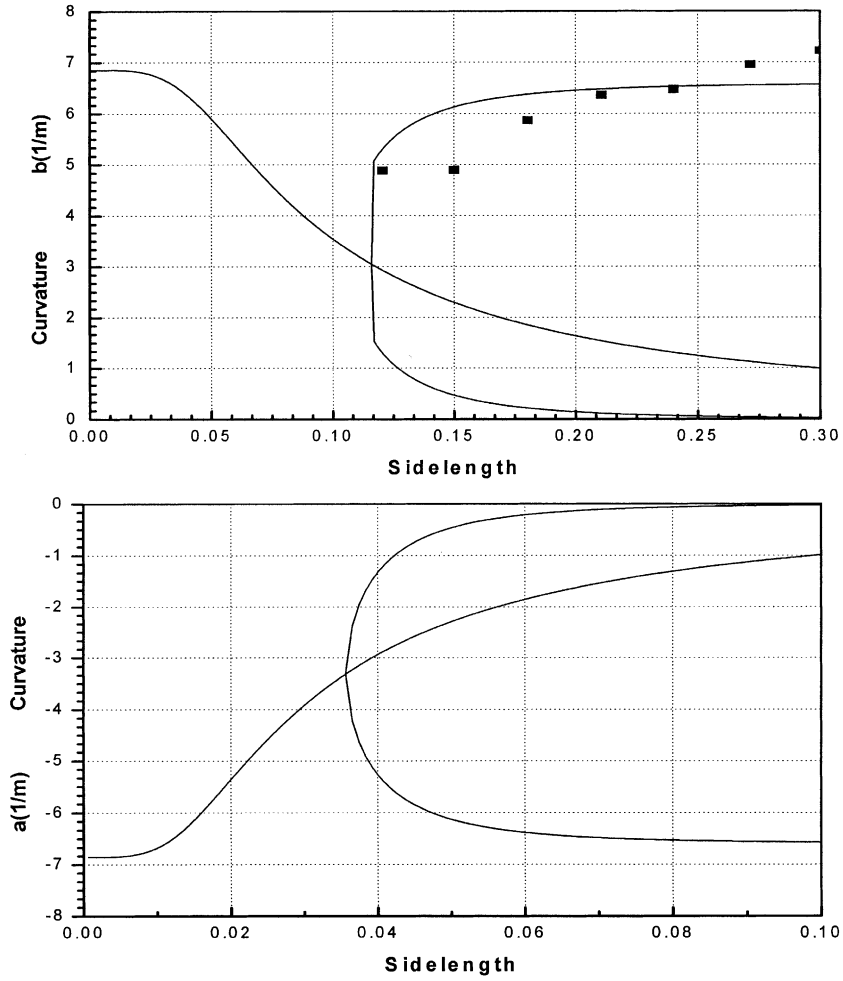

Fig. 11. Change of curvature as a function of the side length for $[0_2/90_2]$ laminate with 0.1×0.3 m (Smooth Al Tool: $\beta_1 = 0.075, \beta_2 = 0.055$) [—: Present, ■: Experiment].

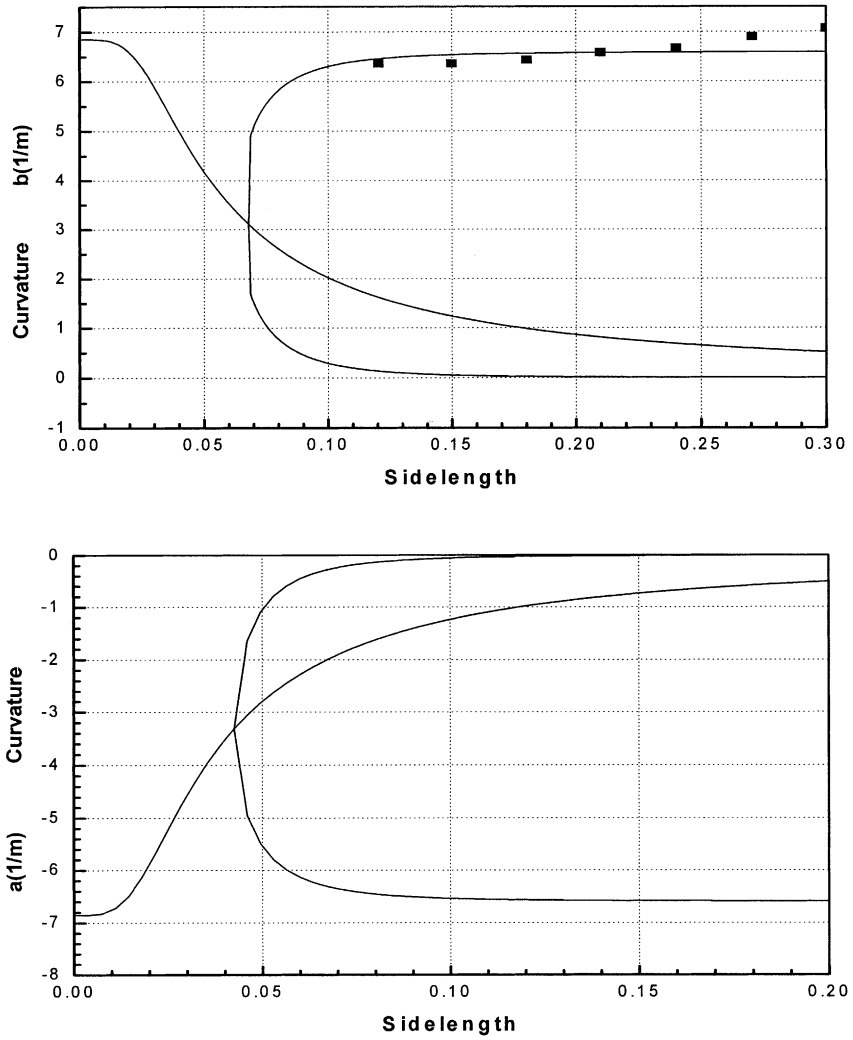

Fig. 12. Change of curvature as a function of the side length for $[0_2/90_2]$ laminate with 0.2×0.3 m (Smooth Al Tool: $\beta_1 = 0.075, \beta_2 = 0.055$) [—: Present, ■: Experiment].

expansion properties of the tool-plate. As the laminate thickness increased, the coefficients β_1 and β_2 increased, which is similar to the behavior displayed by the smooth aluminum tool-plate. When the laminate thickness increased, the slippage coefficient was less sensitive to the type of the tool-plate.

Figs. 10–12 show the change of slippage coefficients and the curvature variations of the laminate plate of various aspect ratios which used the same tool-plate (the smooth aluminum tool). When the aspect ratio was equal to 1 (square plate case), the analytical results including the slippage effects agreed well with experimental results as shown in Fig. 10. Figs. 11 and 12 depict the correlations between the predicted curvature shape and test results as the side lengths were varied at a fixed aspect ratio 1/3 or 2/3, respectively. Figs. 11 and 12 show that the bifurcation point of curvature b appears in the larger side-length as the aspect ratio decreased. The theoretical results obtained from the present model correlated very well with the experimental values. Moreover, the slippage coefficients $\beta_1$and β_2 which matched in square laminates can be used, as they are, in the rectangular laminates of various aspect ratios since the environment effects such as the conditions of curing and tool-plates are the same.

4. Conclusions

A refined analytical model of the curvature shapes of unsymmetric laminates at room-temperature and experimental results were presented. The model accounts for slippage effects. To develop a more accurate model than the one in the previous study [10], we modified the transverse shear stress profile to give a monotonic pattern across the thickness of the laminates and used fifth-order polynomial approximation to derive the laminate mid-plane strains. The asymptotic curvature values of the proposed model were matched to the experimental value at one point; the slippage coefficients were obtained. We observed that the change

of curvature depends on the type of tool-plate and the laminate thickness. The slippage coefficient derived from the square laminates can be directly applied to the rectangular-shape laminates of various aspect ratios for equal layup configurations and same type of tool-plate.

Acknowledgements

This work was supported by the Micro Thermal System Research Center through the Korea Science and Engineering Foundation.

References

[1] Hyer MW. Some observations on the cured shape of thin unsymmetric laminates. J Composite Materials 1981;15:175–94.
[2] Hyer MW. Calculations of the room temperature shape of unsymmetric laminates. J Composite Materials 1981;15:296–310.
[3] Hyer MW. The room-temperature shapes of four-layer unsymmetric cross-ply laminate. J Composite Materials 1982;16:318–40.
[4] Hamamoto A, Hyer MW. Non-linear temperature-curvature relationships for unsymmetric graphite-epoxy laminates. Int J Solids Structures 1987;23:919–35.
[5] Hong CS, Jun WJ. Effect of residual shear strain on the cured shape of unsymmetric cross-ply thin laminates. Comp Sci Tech 1990;38:55–67.
[6] Peeters LJB, Powell PC, Warnet L. Thermally-induced shapes of unsymmetric laminates. J Composite Materials 1996;30:603–26.
[7] Schlecht M, Schulte K, Hyer MW. Advanced calculation of the room-temperature shapes of thin unsymmetric composite laminates. Composite Structures 1995;32:627–33.
[8] Schlecht M, Schulte K. Advanced calculation of the room-temperature shapes of unsymmetric laminates. J Composite Materials 1999;33:1472–90.
[9] Dano M, Hyer MW. Thermally-induced deformation behavior of unsymmetric laminates. Int J Solids Structures 1998;35:2101–20.
[10] Cho M, Kim M, Choi H, Chung C, Ahn K, Eom Y. A study on the room-temperature curvature shapes of unsymmetric laminates including slippage effects. J Composite Materials 1998;32:460–82.
[11] Mathematica Ver. 4.0 Reference guide. Wolfram Research, 2000.